Strojniški vestnik - Journal of Mechanical Engineering 63(2017)11, 657-665
DOI:10.5545/sv-jme.2017.4491
Original Scientific Paper
Received for review: 2017-03-30
Received revised form: 2017-07-18
Accepted for publication: 2017-08-18


# Hysteresis Modelling and Compensation of Pneumatic Artificial Muscles using the Generalized Prandtl-Ishlinskii Model

Jiangping Mei – Shenglong Xie – Haitao Liu* – Jiawei Zang
Tianjin University, Key Laboratory of Mechanism Theory and Equipment Design, China

*The pneumatic artificial muscle (PAM) has attracted extensive attention from both industrial and academic fields due to its high power/weight ratio and significant compliance. However, the inherent hysteresis nonlinearities, including force-length and length-pressure hysteresis, have significant influence on the accuracy of trajectory tracking control. This paper presents a generalized Prandtl-Ishlinskii (GPI) model and its inversion for the asymmetric hysteresis characterization and compensation of the PAM. By using the Levenberg-Marquardt (L-M) method, the parameters in the proposed GPI model are identified, based on which the simulation result of the GPI model and the measured experimental data are compared to validate the identification. To compensate for the nonlinear length-pressure hysteresis, a feedforward/feedback combined control scheme is developed to realize highly accurate trajectory tracking control of the PAM. The experimental results show that the inverse GPI model has a good capability of compensating the asymmetric length-pressure hysteresis.*
**Keywords: hysteresis nonlinearity, generalized Prandtl-Ishlinskii (GPI) model, trajectory tracking control, Levenberg-Marquardt method**

**Highlights**

- *The generalized Prandtl-Ishlinskii model is used to characterize the length-pressure hysteresis of a pneumatic artificial muscle.*
- *The numbers of generalized play operator in the proposed model are much smaller than those in the classical Prandtl-Ishlinskii model.*
- *The Levenberg-Marquardt method shows great efficiency for the identification of the parameters in the proposed model.*
- *The generalized Prandtl-Ishlinskii model can accurately describe the asymmetric hysteresis and has high accuracy in trajectory tracking of the pneumatic artificial muscle.*

## 0 INTRODUCTION

The pneumatic artificial muscle (PAM), also called pneumatic muscle actuator (PMA) or fluidic muscle, is a tube-like pneumatic actuator, which consists of a flexible cylinder rubber surrounded by a braided mesh shell (see Fig. 1) [1].

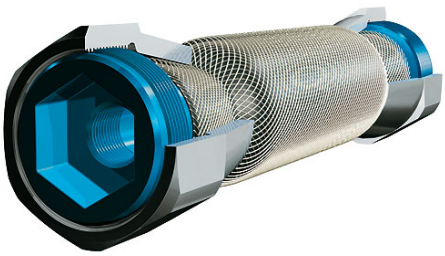

**Fig. 1.** *The pneumatic artificial muscle*

As a tensile actuator, the diaphragm of PAM extends in the circumferential direction when internal pressure is applied, resulting in a tensile force and a contraction motion in the longitudinal direction. The PAM has many advantages, including as simple structure, cleanliness, high power/weight ratio, low cost, etc. More importantly, the compliance [2] of the PAM behaves very similarly to the organic muscle. This characteristic makes it widely used in rehabilitation, medical nursing and agriculture robots [3] and [4]. However, high-accuracy control of a PAM is by no means an easy task, due to the hysteresis phenomenon amongst length, pressure, and force [5], which makes the design of the controller complicated for an accurate trajectory control.

To eliminate the negative effects caused by hysteresis, extensive studies have been witnessed in recent years. The hysteresis models of the PAM can be roughly divided into two classes [6]: operator-based models and differential-based models. Members belonging to the first class use different kinds of mathematical operators to characterize the hysteresis phenomenon, including the Preisach model, Prandtl–Ishlinskii (PI) model and Maxwell-Slip model. Employing the stop operators, Ito et al. [7] and [8] derived the hysteresis model of the PAM to realize the motion control of a parallel manipulator. Minh et al. [1] developed a lumped-parametric quasi-static model based on the Maxwell-slip model to capture the force-length hysteresis, which can be easily used for the control of a PAM. Xie et al. [9] established the PI model to describe the length-pressure hysteresis of a PAM

*Corr. Author's Address: Tianjin University, Key Laboratory of Mechanism Theory and Equipment Design, Weijin Road, Tianjin, 300072, China, liuht@tju.edu.cn

and derived the inverse model for trajectory tracking of a PAM by using fast-switching valves. Kosaki and Sano [10] described the length-pressure hysteresis using the Preisach model for the control of a parallel manipulator driven by three PAMs. The second class is based on the differential equations to characterize the hysteresis, such as the Duhem model, LuGre model, Bouc-Wen model, etc. In a similar manner, Lin et al. [11] investigated the hysteresis modeling and tracking control methods of the PAM by using the Bouc-Wen model, and designed different feedback control schemes for the compensation of hysteresis in order to reduce the tracking errors. Zhao et al. [12] applied the Duhem model to characterize the force-length hysteretic behaviour of the PAM, based on which a novel cascade position PID controller was designed to regulate the pressure. Zhong et al. [13] constructed the force-length hysteresis model in the form of the Bouc-Wen model, and developed a nonlinear PID control scheme to improve the kinematic performance of a manipulator actuated by PAMs. Aschemann and Schindele [14] adopted the generalized Bouc-Wen model, quasi-static Maxwell-slip model, and Prandtl–Ishlinskii model to establish the force-length hysteresis, and concluded that the first model was the most effective one for the control of a high-speed linear axis actuated by PAMs. Among these studies, the PI model is the most widely used due to the following advantages [11]: (1) the PI model contains a limited number of linear play operators; (2) both the PI model and the inverse PI model have analytical expressions. It must be pointed out that the conventional PI model is unable to describe the asymmetric characteristic of the hysteresis [15] and saturation [16], due to the symmetric property of the linear play operators. To solve this problem, asymmetric hysteresis modelling approaches, especially for smart materials, ferromagnetic materials and smart actuators, are intensively studied. Kuhen [17] proposed a modified PI model that combines linear play operators with dead-zone operators, which is capable of describing the asymmetric hysteresis of magnetostrictive actuators. Gu et al. [18] combined the conventional PI model with a nonlinear non-hysteretic function of the input to capture the asymmetric hysteresis of piezoceramic actuators. Janaideh et al. [19] proposed a generalized PI (GPI) model to characterize the saturated symmetric hysteresis loops of smart actuators. Zhang et al. [20] applied the GPI model to successfully describe the asymmetric hysteresis loops of Vanadium dioxide materials. However, few studies show the effectiveness of these variations of the PI model for PAMs except for the investigation carried out by Liu et al. [21], in which a modified PI model was used to describe the asymmetric length-pressure hysteresis.

Drawing on the GPI model, this paper deals with the length-pressure hysteresis modelling and inverse GPI model compensation of PAMs. The rest of this paper is organized as follows. First, the experimental setup for measuring the length-pressure hysteresis and trajectory tracking control of a PAM is briefly introduced, followed by the formulation of the analytical forms of the GPI model and its inversion. Then the parameters in the model are identified using the Levenberg-Marquardt method, and the validation of the model is testified in comparison with the experimental measurements. Finally, an inverse-based compensator for trajectory tracking control of the PAM is designed to demonstrate the effectiveness of the model before conclusions are drawn in Section 5.

## 1 MEASUREMENTS OF THE LENGTH-PRESSURE HYSTERESIS OF A PAM

The experimental setup is shown in Fig. 2, and the components are listed in Table 1.

**Fig. 2.** *Experimental setup*

A PAM (FESTO DMSP-20-500) from FESTO is used for testing, of which one extremity is connected with the base and the other moves freely. The length and the internal pressure of the PAM are measured using a displacement sensor (Novetechnik TEX-0150) and a pressure transducer (FESTO SDE1-D10), respectively. A proportional pressure regulator (Festo VPPM-6L-L-1-G18-0L10H) is equipped to regulate the required pressure for the PAM. Fig. 3 shows the schematic diagram of the experimental setup.

The experimental process is given as follows. Initially, the PAM is at its full length, and the internal

**Table 1.** *Components of the system*

| Component | Type | Parameters | Company |
|---|---|---|---|
| PAM | DMSP-20-500N | Length 500 mm, Diameter 20 mm<br>Maximal permissible contraction 25 % Maximal additional load 80 kg | Festo |
| Proportional pressure regulator | VPPM-6L-L-1-G18-0L10H | Regulator range: 0 to 10 bar, Full scale linearity error ±0.5 %<br>Full scale repetition accuracy 0.5 % | Festo |
| Pressure sensor | SDE1-D10-G2-WQ4-L-PU | Max pressure 10 bar, Full scale accuracy ±2 % | Festo |
| Displacement sensor | TEX-0150-415-002-205 | Measurement range 150 mm, Repeat accuracy ± 0.01 mm | Novetechnik |
| Data acquisition card | PCI-6230 | 8 analogue input, 8 analogue output | NI |

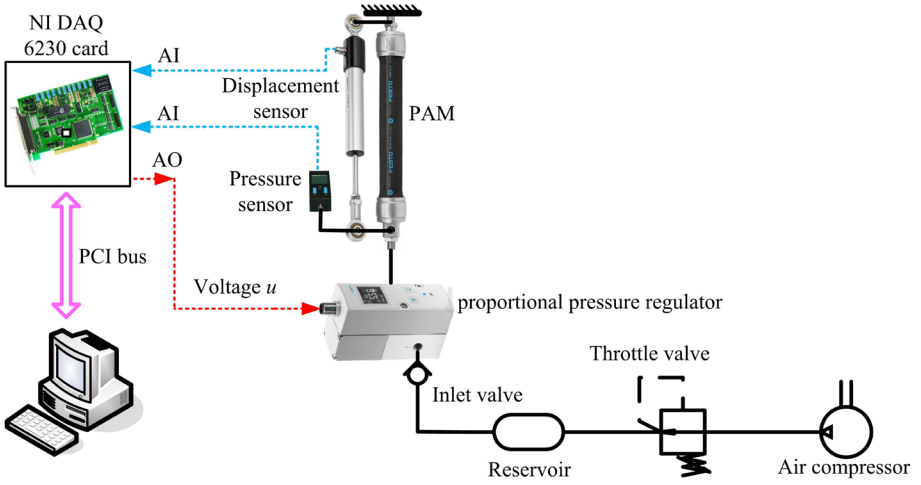


**Fig. 3.** *Configuration of the experimental testing system*

pressure is zero. The reference pressure signal is designed in the form of triangle-wave with a frequency of 0.2 Hz (see Fig. 4). Its amplitude decreases from 0.6 MPa to 0.1 MPa with an equal interval of 0.1 MPa. During the experiment, the contraction and internal pressure of the PAM are recorded. Fig. 5 shows the corresponding length-pressure hysteresis curve of the PAM, from which it can be seen that the major hysteresis loop varies from 0 MPa to 0.6 MPa, and five minor hysteresis loops vary from 0 MPa to 0.5 MPa, 0.4 MPa, 0.3 MPa, 0.2 MPa, and 0.1 MPa, respectively. Obviously, given the same internal pressure, the contraction ratios of the PAM are different in the process of stretching and contraction. The measured data of the major hysteresis loop (see Fig. 5, red line) are used to identify the parameters in

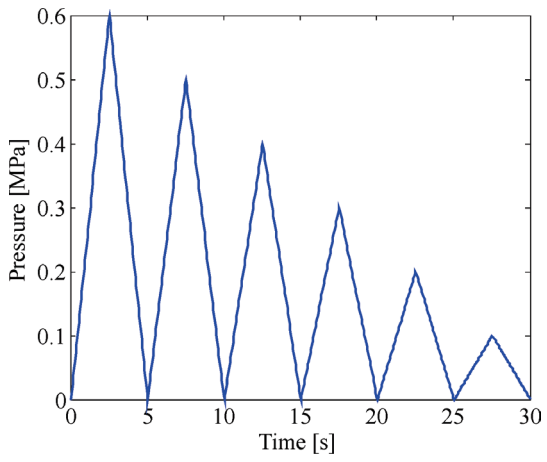


**Fig. 4.** *The referenced input signal of pressure*

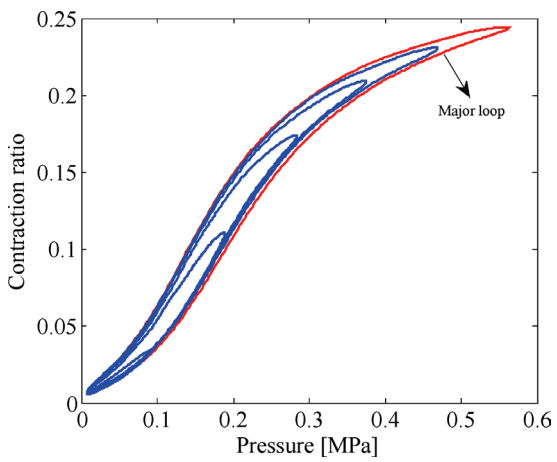


**Fig. 5.** *Length/Pressure hysteresis of PAM*

the GPI model that will be derived in the following section.

## 2 LENGTH-PRESSURE HYSTERESIS MODELLING

The analytical formulations of the GPI model and its inverse model are presented in this section. The former is used to characterize the length-pressure hysteresis, while the latter is applied as a feedforward compensator for trajectory tracking control.

### 2.1 The Classical PI Model

The classical PI model is a linearly weighted superposition of elementary play operators with different thresholds and weighting values. The input-output relationship of a linear play operator is illustrated in Fig. 6. Its envelop function is a straight line with a slope of one. Fig. 7 shows the superposition of a finite number of linear play operators to characterize the hysteresis in the discrete space. The expression of the ith linear play operator can be formulated as [22]:

$$y_i(k) = \max\left\{x(k) - r_i, \min\left\{x(k) + r_i, y_i(k-1)\right\}\right\}, \quad (1)$$

while the initial condition is:

$$y_i(0) = \max\left\{x(0) - r_i, \min\left\{x(0) + r_i, y_{i0}\right\}\right\}. \quad (2)$$

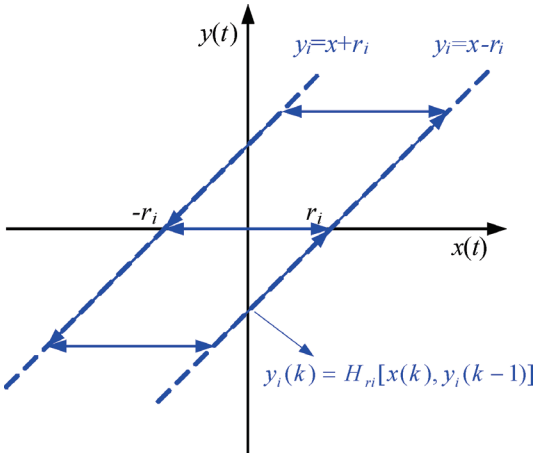


**Fig. 6.** *The linear play operator*

The output of the PI model can be written as:

$$y_p(k) = \sum_{i=1}^{n} \omega_i y_i(k) = \boldsymbol{\omega}^T \boldsymbol{H}_r[x(k), \boldsymbol{y}_0] \quad (3)$$

where $\boldsymbol{H}_r$ denotes the linear play operator; $\boldsymbol{\omega} = [\omega_1, ..., \omega_n]^T$ is the weighting vector; $\boldsymbol{r} = [r_1, ..., r_n]^T$ is the threshold vector; $x$ and $y$ are the input and output of the operator, respectively; $y_0$ is the initial state; $n$ is the number of play operators. It has been shown that the conventional PI model cannot characterize asymmetric hysteresis loops of the PAM [21].

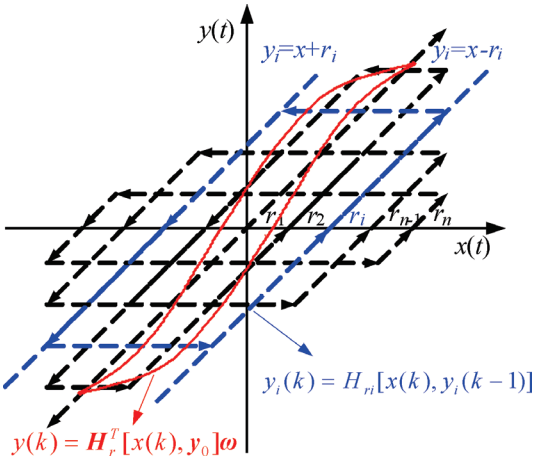


**Fig. 7.** *The PI model*

### 2.2 The Generalized PI Model

Due to the limitations of the conventional PI model, the GPI model [23] is employed to describe the length-pressure hysteresis behaviour of a PAM. The GPI model is expressed as a weighted superposition of generalized play operators. The input-output relationship of a generalized play operator is shown in Fig. 8. The $i^{th}$ generalized play operator can be mathematically expressed as:

$$y_i(k) = \max\left\{\gamma[x(k)] - r_i, \min\left\{\gamma[x(k)] + r_i, y_i(k-1)\right\}\right\}, \quad (4)$$

where $\gamma[x(k)]$ is the envelop function of the generalized play operator. In this paper, the hyperbolic-tangent function is chosen to describe the output saturation under certain input, such that the envelop function can be given by:

$$\gamma = c_0 \tanh[c_1 x(k) + c_2] + c_3, \quad (5)$$

where $c_0 > 0$, $c_1 > 0$, $c_2$, $c_3$ are constants to be identified. Thus, the GPI model can be formulated as:

$$y_P(k) = q\gamma[x(k)] + \sum_{i=1}^{n} p(r_i) y_i(k), \quad (6)$$

where $q$ is a positive constant. According to [23], the threshold value $r_i$ and the weight of the $i^{th}$ operator $p(r_i)$ are given as:

$$r_i = \alpha i, \quad (7)$$

$$p(r_i) = \rho e^{-\tau r_i}, \tag{8}$$

where $\alpha$, $\rho$ and $\tau$ are positive constants that need to be identified from experimental data.

Moreover, the inverse of the GPI model can be analytically expressed as:

$$x_p(k) = \gamma^{-1}\left(q'y(k) + \sum_{i=1}^{n} p_i' x_i(k)\right), \tag{9}$$

where the parameters in this model can be obtained following the conventional PI model and given as

$$x_i(k) = \max\left\{y(k) - r_i', \min\left\{y(k) + r_i', x_i(k-1)\right\}\right\}, \tag{10}$$

$$\begin{cases} q' = \dfrac{1}{q} \\ r_i' = qr_i + \displaystyle\sum_{j=1}^{i-1} p_j\left(r_i - r_j\right) \\ p_i' = \dfrac{-p_i}{\left(q + \displaystyle\sum_{j=1}^{i} p_j\right)\left(q + \displaystyle\sum_{j=1}^{i-1} p_j\right)} \end{cases}, \tag{11}$$

where $x_i(k)$ is the $i^{\text{th}}$ inverse generalized linear play operator; $r_i'$ and $p_i'$ represent the $i^{\text{th}}$ threshold and weight, respectively.

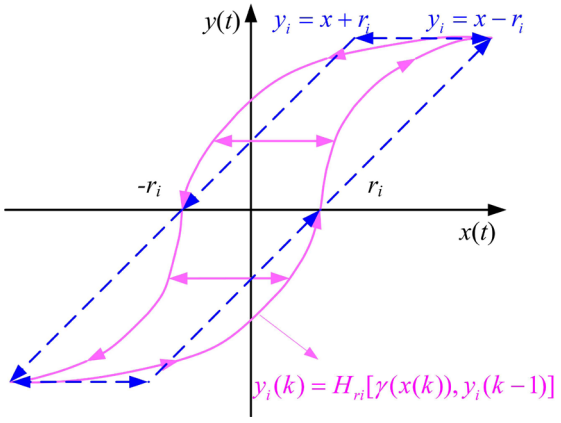


**Fig. 8.** *The generalized play operator*

## 3 PARAMETER IDENTIFICATION

In this section, the Levenberg-Marquardt (L-M) method is used to identify the parameters in the GPI model. Then the identified model is validated by comparing the simulation result and measured data.

### 3.1 The Levenberg-Marquardt Method

The nonlinear least-squares algorithm is a widely used technique in parameter estimation, which can be used to find the coefficients by minimizing a weighted cost function of the measured data. For this specific case, the following quadratic cost function is formulated:

$$\boldsymbol{F} = \boldsymbol{E}^{\mathrm{T}}(\boldsymbol{\Theta})\boldsymbol{E}(\boldsymbol{\Theta}) = \sum_{k=1}^{N}\left(y_t(k) - y_p(k,\boldsymbol{\Theta})\right)^2, \tag{12}$$

subject to

$$\begin{cases} y_p(k,\boldsymbol{\Theta}) = q\gamma[x_t(k)] + \displaystyle\sum_{i=1}^{n} p(r_i) y_i(k) \\ c_0 > 0, c_1 > 0, \rho > 0, \tau > 0 \end{cases}, \tag{13}$$

where $\boldsymbol{\Theta} = [c_0, c_1, c_2, c_3, q, \rho, \tau, \alpha]^{\mathrm{T}}$ is a set of identified parameters in the GPI model; $\boldsymbol{E}(\boldsymbol{\Theta})$ is the error vector; $x_t$ and $y_t$ are input and output data obtained from the experiment; $N$ is the number of $x_t$; $y_p$ is the output of the GPI model. The identification process can be expressed as [24]:

$$\boldsymbol{\Theta}_{k+1} = \boldsymbol{\Theta}_k - \boldsymbol{H}_k^{-1}\boldsymbol{J}_k^{\mathrm{T}}\boldsymbol{E}_k, \tag{14}$$

where $\boldsymbol{H}_k$ is the Hessian matrix, which is a square matrix of second-order partial derivatives of the error vector $\boldsymbol{E}$ with respect to the parameter vector $\boldsymbol{\Theta}$; $\boldsymbol{J}_k$ is the Jacobian matrix that can be presented as:

$$\boldsymbol{J}_k = \begin{bmatrix} \dfrac{\partial E_1}{\partial \Theta_1} & \dfrac{\partial E_1}{\partial \Theta_2} & \cdots & \dfrac{\partial E_1}{\partial \Theta_n} \\ \dfrac{\partial E_2}{\partial \Theta_1} & \dfrac{\partial E_2}{\partial \Theta_2} & \cdots & \dfrac{\partial E_2}{\partial \Theta_n} \\ \vdots & \vdots & \cdots & \vdots \\ \dfrac{\partial E_m}{\partial \Theta_1} & \dfrac{\partial E_m}{\partial \Theta_2} & \cdots & \dfrac{\partial E_m}{\partial \Theta_n} \end{bmatrix},$$

$$\boldsymbol{E}_k = y_t(k) - y_p(k,\boldsymbol{\Theta}) = [E_1, E_2 \cdots, E_n]^{\mathrm{T}},$$

where $E_i$ is the error between the $i^{\text{th}}$ output of the GPI model and the output data obtained from the experiment; $\Theta_i$ is the $i^{\text{th}}$ parameter of vector $\boldsymbol{\Theta}$; and $n = 1$ for this particular case.

In order to improve the convergence of the solution, the Hessian matrix in Eq. (14) is expressed by:

$$\boldsymbol{H}_k = \boldsymbol{J}_k^{\mathrm{T}}\boldsymbol{J}_k + \mu\boldsymbol{I}, \tag{15}$$

where $\mu$ is called the combination coefficient, which is a damping parameter to approximate the Hessian matrix; $\boldsymbol{I}$ is the identity matrix, which is applied to guarantee the approximated Hessian matrix to be

invertible all the time. Then, substituting Eq. (15) into Eq. (14) yields [25]:

$$\boldsymbol{\Theta}_{k+1} = \boldsymbol{\Theta}_k - \left(\boldsymbol{J}_k^{\mathrm{T}}\boldsymbol{J}_k + \mu\boldsymbol{I}\right)^{-1}\boldsymbol{J}_k^{\mathrm{T}}\boldsymbol{E}_k, \qquad (16)$$

which represents the parameter vector updating rule in each iteration. By using this method, the problem will converge to the optimal solution [24].

Table 2 lists the identified parameters of the GPI model (Eq. (6)) with ten generalized play operators ($n$=10). Fig. 9 shows the comparison of the outputs of the identified GPI model with the measured data. It can be seen that the GPI model is effective in characterizing the asymmetric length-pressure hysteresis loops of the PAM.

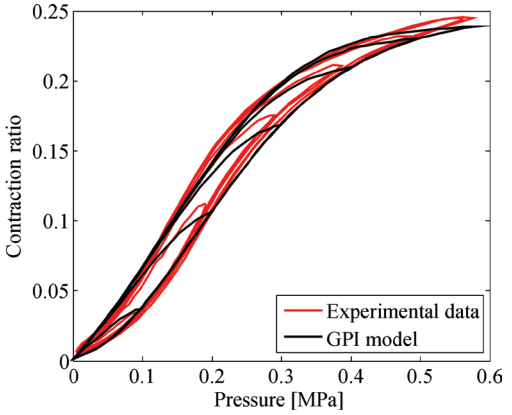


**Fig. 9.** *Model validation result of the GPI model*

**Table 2.** *Identified parameters*

| $c_0$ | $c_1$ | $c_2$ | $c_3$ |
|---|---|---|---|
| 1.428 | 0.418 | -0.604 | 0.637 |
| $q$ | $\rho$ | $\tau$ | $\alpha$ |
| 0.047 | 0.042 | 5.001 | 0.08 |

## 4 INVERSE GPI MODEL FOR COMPENSATION IN POSITION CONTROL OF PAM

To compensate the length-pressure hysteresis, a feedforward/feedback combined control strategy is developed to realize highly accurate trajectory tracking control of the PAM. The feedforward compensator is designed based on the inverse GPI model in order to reduce the influence of length-pressure hysteresis, while the feedback controller is used to overcome the tracking error caused by creep and vibrations.

### 4.1 Control Scheme

Given the identified parameters of the GPI model, the inverse GPI model can be obtained using Eqs. (9) to (11), which is then cascaded with the control system as a feedforward hysteresis compensator. The inverse GPI model maps the desired trajectory $y_d$ into a desired control input signal $P_d$ applied to the proportional pressure regulator. Hence, the relationship between the desired trajectory $y_d$ and actual length $y_r$ can be linearized. Note that the accuracy of the hysteresis model affects the performance of the feedforward controller. Therefore, a feedback loop must be added to form a feedforward/feedback combined controller. The control scheme is illustrated in Fig. 10. In this paper, a conventional PID controller is included in the feedback loop, which has the following form:

$$\Delta P = K_p e(t) + K_i \int_0^t e(\tau)d\tau + K_d \frac{de(t)}{dt}, \qquad (17)$$

where $e(t)$ is the tracking error signal; $\Delta P$ is the output of PID controller; $K_p$, $K_i$, and $K_d$ are proportional, integral, and derivative gains, respectively, which are given in Table 3.

**Table 3.** *Parameters of PID controller*

| $K_p$ | $K_i$ | $K_d$ |
|---|---|---|
| 0.05 | 0.01 | 0 |

### 4.2 Experimental Results

To testify regarding the performance of the proposed control scheme, an experiment on trajectory tracking

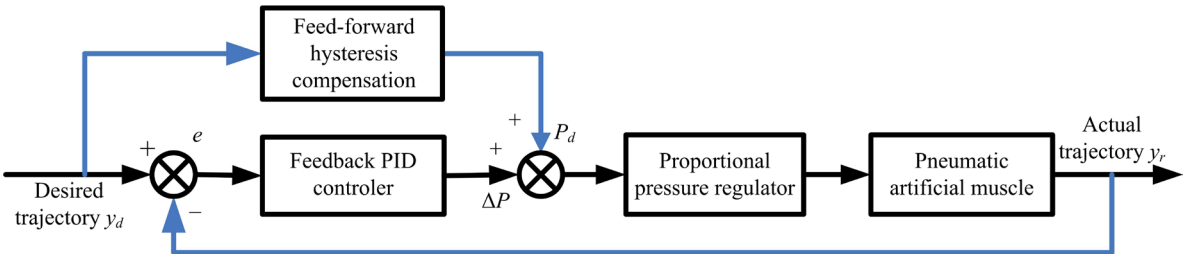


**Fig. 10.** *Feedforward/feedback combined control scheme for pneumatic artificail muscle*

control of the PAM is implemented. The desired sinusoidal tracking signal is designed as:

$$y_d(t) = A\sin\left(2\pi ft + \varphi\right) + L, \tag{18}$$

where $y_d(t)$ is the desired trajectory signal output; $A$ is the amplitude and $\varphi$ is the initial phase; $f$ and $L$ are the frequency and offset of the desired signal, respectively. Table 4 gives the parameters in Eq. (18).

**Table 4.** *Parameters of sinusoidal signal*

| $A$ [mm] | $f$ [Hz] | $\varphi$ [rad] | $L$ [mm] |
|---|---|---|---|
| 45 | 0.2 | $\pi/2$ | 450 |

**Table 5.** *The tracking error of sinusoid trajectory*

| Maximum error [mm] | Mean absolute error [mm] | RMS error [mm] |
|---|---|---|
| 2.659 | 0.7358 | 0.8701 |

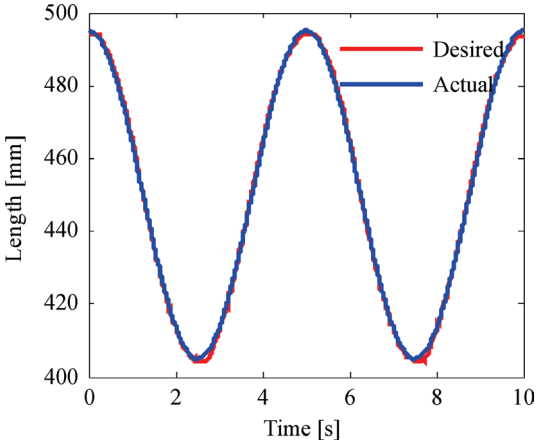


**Fig. 11.** *Trajectory tracking responses*

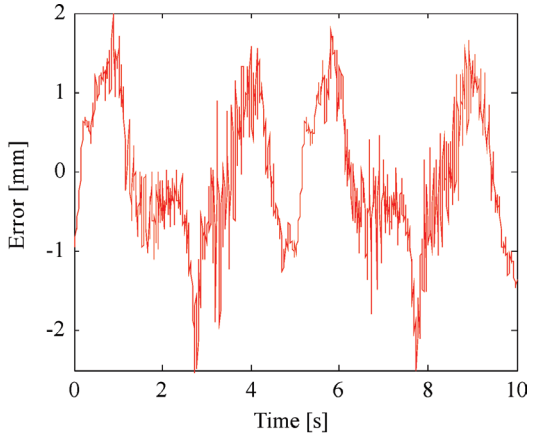


**Fig. 12.** *Trajectory tracking errors*

The tracking responses and errors of the proposed control scheme are shown in Figs. 11 and 12, respectively. Table 5 lists the statistics of the trajectory tracking error. Numerical results show that the maximal error is 2.659 mm, and the mean absolute error is only 0.7358 mm. From the experimental results, it can be concluded that the inverse GPI model is very effective to compensate the effects of length-pressure hysteresis in real-time application. This conclusion can also be drawn from the nearly linear relationship between the desired and the actual lengths of the PAM after compensation (see Fig. 13).

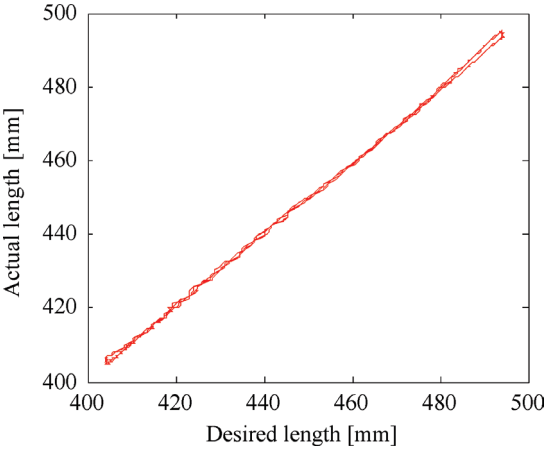


**Fig. 13.** *Relationship between the desired length and the actual length after compensation*

## 5 CONCLUSIONS

To capture the asymmetric length-pressure hysteresis of the PAM, a generalized Prandtl-Ishlinskii (GPI) model and its inverse model are presented in this paper. Compared to the classical Prandtl-Ishlinskii (CPI) model, the proposed GPI model utilizes the hyperbolic-tangent function as the envelope function of generalized play operators to characterize the asymmetric hysteresis loops. The parameters in the GPI model are identified by using the Levenberg-Marquardt method, making the process of identification convenient and efficient. Based on the inverse GPI model, a feedforward/feedback combined control scheme is developed to compensate the length-pressure hysteresis nonlinearity and realize high accurate trajectory tracking control of the PAM. The experimental results show that the proposed GPI model and its inversion are effective for describing the asymmetric length-pressure hysteresis of the PAM in terms of both major and minor hysteresis loops. However, since the symmetric envelop function is used in the generalized play operator, the capability of this model in characterizing the asymmetric hysteresis loops is limited. Therefore, the feedback controller

combined with the asymmetric GPI model-based feedforward compensator will be investigated in future work to further improve the trajectory tracking performance.

## 6 ACKNOWLEDGEMENTS

This work is supported by National Natural Science Foundation of China under Grant 51405331.

## 7 NOMENCLATURE

$x$ the input of the linear play operator or generalize play operator, [mm]
$y$ the output of the linear play operator or generalize play operator, [%]
$n$ the number of the linear play operator or generalize play operator
$y_i$ the $i^{\text{th}}$ linear play operator or generalize play operator, [%]
$y_p$ the output of PI or GPI model, [%]
$\omega$ the weighting vector of PI model
$\boldsymbol{r}$ the threshold vector of PI model
$\boldsymbol{y}_0$ the initial state of the linear play operator or generalize play operator
$x_p$ the output of inverse GPI model, [MPa]
$x_i$ the $i^{\text{th}}$ inverse generalize play operator
$r_i'$ the $i^{\text{th}}$ threshold of the inverse GPI model
$p_i'$ the $i^{\text{th}}$ weight of the inverse GPI model
$\gamma$ the envelope function of the generalize play operator
$c_0$ the constants of envelop function in GPI model
$c_1$ the constants of envelop function in GPI model
$c_2$ the constants of envelop function in GPI model
$c_3$ the constants of envelop function in GPI model
$q$ a positive constant of GPI model
$r_i$ the threshold value of the $i^{\text{th}}$ generalize play operator
$p(r_i)$ the weight of the $i^{\text{th}}$ generalize play operator
$\alpha$ the positive constant of $r_i$
$\rho$ the positive constant of $p(r_i)$
$\tau$ the positive constant of $p(r_i)$
$\boldsymbol{F}$ the quadratic cost function
$\boldsymbol{\Theta}$ identified parameter vector in GPI model
$\boldsymbol{E}$ the error vector
$x_t$ the input data obtained from experiment, [mm]
$y_t$ the output data obtained from experiment, [%]
$N$ the number of $x_t$
$\boldsymbol{H}_k$ the Hessian matrix, second-order partial derivatives of the error vector $\boldsymbol{E}$ with respect to the parameter vector $\boldsymbol{\Theta}$
$\boldsymbol{J}_k$ the Jacobian matrix of the error vector $\boldsymbol{E}$ with respect to the parameter vector $\boldsymbol{\Theta}$
$\mu$ the combination coefficient
$\boldsymbol{I}$ the identity matrix
$e(t)$ the tracking error signal, [mm]
$\Delta P$ the output of PID controller, [V]
$K_p$ the proportional gain
$K_i$ the integral gain
$K_d$ the derivative gain
$y_r$ the actual trajectory, [mm]
$P_d$ the desired control input signal, [V]
$y_d$ the desired trajectory signal, [mm]
$A$ the amplitude of $y_d$, [mm]
$f$ the frequency of $y_d$, [Hz]
$\varphi$ the initial phase of $y_d$, [rad]
$L$ the offset of $y_d$, [mm]

## 8 REFERENCES

[1] Minh, T.V., Tjahjowidodo, T., Ramon, H., Van Brussel, H. (2011). A new approach to modeling hysteresis in a pneumatic artificial muscle using the Maxwell-slip model. *IEEE/ASME Transactions on Mechatronics*, vol. 16, no. 1, p. 177-186, **DOI:10.1109/TMECH.2009.2038373**.

[2] Daerden, F., Lefeber, D. (2002). Pneumatic artificial muscles: actuators for robotics and automation. *European Journal of Mechanical and Environmental Engineering*, vol. 47, no. 1, p. 11-21.

[3] Tondu, B., Ippolito, S., Guiochet, J., Daidie, A. (2005). A seven-degrees-of-freedom robot-arm driven by pneumatic artificial muscles for humanoid robots. *The International Journal of Robotics Research*, vol. 24, no. 4, p. 257-274, **DOI:10.1177/0278364905052437**.

[4] Yeh, T.J., Wu, M.J., Lu, T.J. (2010). Control of McKibben pneumatic muscles for a power-assist, lower-limb orthosis. *Mechatronics*, vol. 20, no. 6, p. 686-697, **DOI:10.1016/j.mechatronics.2010.07.004**.

[5] Minh, T.V., Kamers, B., Tjahjowidodo, T., Ramon, H., Van Brussel, H. (2010). Modeling torque-angle hysteresis in a pneumatic muscle manipulator. *Proceedings of the IEEE/ASME International Conference on Advanced Intelligent Mechatronics*, p. 1122-1127, **DOI:10.1109/AIM.2010.5695805**.

[6] Hassani, V., Tjahjowidodo, T., Do, T.N. (2014). A survey on hysteresis modeling, identification and control. *Mechanical Systems and Signal Processing*, vol. 49, no. 1-2, p. 209-233, **DOI:10.1016/j.ymssp.2014.04.012**.

[7] Ito, A., Kiyoto, K., Furuya, N. (2010). Motion control of parallel manipulator using pneumatic artificial actuators. *Proceedings of IEEE International Conference on Robotics and Biomimetics*, p. 460-465, **DOI:10.1109/ROBIO.2010.5723370**.

[8] Ito, A., Washizawa, N., Kiyoto, K., Furuya, N. (2011). Control of pneumatic actuator in consideration of hysteresis characteristics. *Proceedings of IEEE International Conference on Robotics and Biomimetics*, p. 2541-2546, **DOI:10.1109/ROBIO.2011.6181687**.

[9] Xie, S.L, Mei, J.P., Liu H.T., Wang, P.F. (2017). Motion control of pneumatic muscle actuator using fast switching valve. *Mechanism and Machine Science, Proceedings of ASIAN*

*MMS & CCMMS*. p. 1439-1451, **DOI:10.1007/978-981-10-2875-5_114**.

**[10]** Kosaki, T., Sano, M. (2011). Control of a parallel manipulator driven by pneumatic muscle actuators based on a hysteresis model. Journal of Environment and Engineering, vol. 6, no. 2, p. 316-327, **DOI:10.1299/jee.6.316**.

**[11]** Lin, C.J., Lin, C.R., Yu, S.K., Chen, C.T. (2015). Hysteresis modeling and tracking control for a dual pneumatic artificial muscle system using Prandtl–Ishlinskii model. *Mechatronics*, vol. 28, no. 6, p. 35-45, **DOI:10.1016/j.mechatronics.2015.03.006**.

**[12]** Zhao, J., Zhong, J., Fan J.Z. (2015). Position control of a pneumatic muscle actuator using RBF neural network tuned PID controller. *Mathematical Problems in Engineering*, vol. 2015, art. ID. 810231, **DOI:10.1155/2015/810231**.

**[13]** Zhong, J., Fan, J.Z, Zhu, Y.H, Zhao, J., Zhai, W.J (2014). One nonlinear PID control to improve the control performance of a manipulator actuated by a pneumatic muscle actuator. *Advances in Mechanical Engineering*, vol. 2014, art. ID. 172782, **DOI:10.1155/2014/172782**.

**[14]** Aschemann, H., Schindele, D. (2014). Comparison of model-based approaches to the compensation of hysteresis in the force characteristic of pneumatic muscles. *IEEE Transactions on Industrial Electronics*, vol. 61, no. 7, p. 3620-3629, **DOI:10.1109/TIE.2013.2287217**.

**[15]** Zhang, J., Merced, E., Sepúlveda, N., Tan, X.B (2015). Optimal compression of generalized Prandtl-Ishlinskii hysteresis models. *Automatica*, vol. 57, p. 170-179, **DOI:10.1016/j.automatica.2015.04.012**.

**[16]** Janaideh, M.A., Rakheja, S., Su, C.Y. (2011). An analytical generalized Prandtl–Ishlinskii model inversion for hysteresis compensation in micropositioning control. *IEEE/ASME Transactions on Mechatronics*, vol. 16, no. 4, p. 734-744, **DOI:10.1109/TMECH.2010.2052366**.

**[17]** Kuhnen, K. (2003). Modeling, identification and compensation of complex hysteretic nonlinearities: A modified Prandtl-Ishlinskii approach. *European Journal of Control*, vol. 9, no. 9, p. 407-418, **DOI:10.3166/ejc.9.407-418**.

**[18]** Gu, G.Y., Zhu, L.M., Su, C.Y. (2014). Modeling and compensation of asymmetric hysteresis nonlinearity for piezoceramic actuators with a modified Prandtl–Ishlinskii model. *IEEE Transactions on Industrial Electronics*, vol. 61, no. 3, p. 1583-1595, **DOI:10.1109/TIE.2013.2257153**.

**[19]** Janaideh, M.A. , Mao, J, Rakheja, S., Xie, W., Su, C.Y. (2008). Generalized Prandtl-Ishlinskii hysteresis model: Hysteresis modeling and its inverse for compensation in smart actuators. *Proceedings of IEEE Conference on Decision and Control*, p. 5182-5187, **DOI:10.1109/CDC.2008.4739202**.

**[20]** Zhang, J., Merced, E., Sepúlveda, N., Tan, X.B (2013). Optimal compression of a generalized Prandtl-Ishlinskii operator in hysteresis modeling. *Proceedings of ASME Dynamic Systems and Control Conference*, p. V003T36A005-V003T36A005, **DOI:10.1115/DSCC2013-3969**.

**[21]** Liu, Y.X., Zang, X.Z, Lin, Z.K., Liu X.Y. (2017). Modelling length/pressure hysteresis of a pneumatic artificial muscle using a modified Prandtl-Ishlinskii model. *Strojniški vestnik - Journal of Mechanical Engineering*, vol. 63, no. 1, p. 56-64, **DOI:10.5545/sv-jme.2016.4027**.

**[22]** Kuhnen, K., Janocha, H. (2001). Inverse feedforward controller for complex hysteretic nonlinearities in smart-material systems. *Control and Intelligent Systems*, vol. 29, no. 3, p. 74-83.

**[23]** Janaideh, M.A., Rakheja, S., Su, C.Y. (2009) A generalized Prandtl-Ishlinskii model for characterizing the hysteresis and saturation nonlinearities of smart actuators. *Smart Materials & Structures*, vol. 18, no. 4, p. 1-9, **DOI:10.1088/0964-1726/18/4/045001**.

**[24]** Li, M., Wu, H. Wang, Y., Handroos, H., Carbone, G. (2017). Modified Levenberg–Marquardt Algorithm for Backpropagation Neural Network Training in Dynamic Model Identification of Mechanical Systems. *Journal of Dynamic Systems, Measurement, and Control*, vol. 139, no. 3, p. 1-14, **DOI:10.1115/1.4035010**.

**[25]** Yamashita, N., Fukushima, M. (2001). On the rate of convergence of the levenberg-marquardt method. *Computing Supplementa*, vol. 15, no. 1, p. 239-249, **DOI:10.1007/978-3-7091-6217-0_18**.